

See discussions, stats, and author profiles for this publication at: <https://www.researchgate.net/publication/260530730>

Analysis of land use/land cover change, population shift, and their effects on spatiotemporal patterns of urban heat islands in...

Article *in* Applied Geography · January 2013

CITATIONS

4

READS

378

1 author:

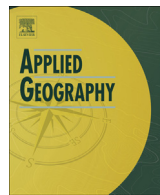


Hao Zhang

Fudan University

22 PUBLICATIONS 61 CITATIONS

[SEE PROFILE](#)



Analysis of land use/land cover change, population shift, and their effects on spatiotemporal patterns of urban heat islands in metropolitan Shanghai, China

Hao Zhang ^a, Zhi-fang Qi ^a, Xin-yue Ye ^b, Yuan-bin Cai ^{a,c}, Wei-chun Ma ^{a,*}, Ming-nan Chen ^a

^a Department of Environmental Science and Engineering, Fudan University, 220 Handan road, Shanghai 200433, China

^b Department of Geography, Kent State University, Kent, OH 44242, USA

^c Fuzhou Research Academy of Environmental Sciences, 32 Jinjishan Road, Fuzhou 350011, Fujian Province, China



ABSTRACT

Keywords:

Land use
Developed land expansion
Population shift
Urban heat island (UHI)
Spatiotemporal patterns
Shanghai
China

Using time series Landsat TM/ETM+ imagery and demographic data of Shanghai for 1997 and 2008, the relationship between land use/land cover (LULC) change and population shift and their effects on the spatiotemporal patterns of urban heat islands (UHIs) were quantitatively examined using an integrated approach of remote sensing, geographical information systems (GIS), and statistical analysis. The results showed that this city has experienced unprecedented urban growth and sprawl during the study period. The developed land increased by 219.50%, approximately 72.52% of which was converted from former cropland (24.79%), fallow land (21.21%), forest and shrub (18.97%), bare land (6.62%), and water (0.93%). Furthermore, in combination with the detection of LULC change, an analysis of the spatially differential growth rates for developed land area and population size revealed an urban–suburban–exurban gradient pattern of population shifting, as evidenced by a sharp increase in developed land area within the middle sub-zones at the urban fringe and the exurban sub-zones beyond the outer traffic ring. Consequently, changes in LULC and population shifts resulted in significant variation in the spatiotemporal patterns of the UHIs due to the loss of water bodies and vegetated surfaces. In the foreseeable future, substantial population growth and urban expansion will continue, especially in the rapidly urbanizing suburban and exurban areas, and thus, the extent and magnitude of UHI effects will continue expanding as well. The relationships between land use, the UHI effect, and regional climate change require that the underlying mechanisms, patterns, and processes of land conversion as well as the response of urban climate should be addressed throughout official decision-making processes. Thus, the planners and decision-makers could fully evaluate the environmental consequences of different land development scenarios and therefore improve the scientific basis of future planning and regulations.

© 2013 Elsevier Ltd. All rights reserved.

Introduction

It is estimated that more than 50% of the global population lives in urban areas, and this percentage will reach 69.6% by 2050 (United Nations, 2010). Currently, urbanization is considered the most important driver of climate change (McCarthy, Best, & Betts, 2010), although the total urban area accounts for only a small proportion of the planetary surface (Grimm, Grove, Pickett, & Redman, 2000; Grübler, 1994). As addressed in previous studies,

intensive and rapid urbanization is an example of human-induced land use/land cover (LULC) change, which has exacerbated the ongoing impacts on the climate system (Jin, Dickinson, & Zhang, 2005). Changes ranging from multi-scale factors such as micro-climatology, biophysical features of underlying surface, urban form and size, and population density played key roles in modifying the local and regional climate (Oke, 1982; Stone, Hess, & Frumkin, 2010). Thus, understanding the influences of urban LULC change on the climate system is of interest in the context of global warming (Trenberth et al., 2007).

Among many useful indices that interpret the relationship between urbanization and climate change, the most well-known and familiar manifestation of urban climate modification is the urban

* Corresponding author. Tel.: +86 21 55665632 (office).

E-mail address: wcma@fudan.edu.cn (W.-c. Ma).

heat island (UHI) (Souch & Grimmond, 2006; Yow, 2007), which is closely linked with urban air quality (Han et al., 2009), energy consumption (Kolokotroni, Giannitsaris, & Watkins, 2006), and population health risk (Hattis, Ogneva-Himmelberger, & Ratick, 2012; Johnson, Stanforth, Lulla, & Luber, 2012). In addition to large-scale weather conditions, the UHI is generally regarded as a local- or meso-scale climatic phenomenon associated with human activities (Zhou & Zhang, 1985). To date, to give a spatially continuous view of the UHI induced by human activities, a combination of in-situ data from meteorological station networks and satellite thermal data is beneficial to understand the processes and mechanisms of the UHI associated with land use/land cover (LULC) change (Stathopoulou & Cartalis, 2007). Traditionally, the atmospheric UHI was measured using fine-scale data, in particular the data from meteorological station sites founded by Luke Howard in the 1900s, the early years of meteorology (Zhou & Zhang, 1985). Unfortunately, it is somewhat difficult to recognize spatial patterns of the UHI with in-situ observational data due to their limited spatial coverage and poor spatial resolution (Streutker, 2003). As an alternative, with recent progress in the field of earth observation, satellite-based remote sensing has been a promising approach to monitor patterns of UHIs at meso and large scales, although the temporal resolution of satellite thermal data is less than that of meteorological observation data. This use of satellite thermal data has been possible and practical since it was first used to study UHIs in the 1970s (Rao, 1972). Since then, high spatial resolution satellite thermal data acquired in the daytime have been widely used to detect surface UHIs on meso or large scales when heat island intensities are greatest (Roth, Oke, & Emery, 1989). More recent studies have validated the successful application of various satellite thermal infrared (TIR) data with varying spatial resolutions, including AVHRR (8 km), MODIS (1 km), HJ-1 B (300 m), Landsat TM (120 m), ASTER (90 m), and Landsat ETM+ (60 m), due to their economical low cost, advantageous spatial coverage, and temporal repetition (Aniello, Morgan, Busbey, & Newland, 1995; Chen, Zhao, Li, & Yin, 2006; Dousset & Gourmelon, 2003; Jusuf, Wong, Hagen, Anggoro, & Hong, 2007; Lo & Quattrochi, 2003; Pongrácz, Bartholy, & Dezsó, 2010; Yang, Gong, Zhou, Huang, & Wang, 2010; Yue, Liu, Ye, & Wu, 2012; Zhou, Zhou, Ge, & Ding, 2001).

Among these available remotely sensed data, the Landsat TM/ETM+ data have been widely used in many case studies of UHIs worldwide (Srivastava, Majumdar, & Bhattacharya, 2009; Stathopoulou & Cartalis, 2007; Weng, 2001; Xian & Crane, 2006), given the free open-access for data acquisition, the long time span, and the spatial coverage for most of the UHI hotspot areas. Moreover, compared with the coarse resolution TIR data, such as AVHRR and MODIS, the recognition of UHIs based on Landsat TM/ETM+ data can produce persuasive results with much greater accuracy. Previous case studies have provided a wealth of useful information, which has allowed us to rethink the adverse consequences of LULC change and rapid urbanization and to therefore help the decision-makers develop and execute rational land use policies. However, studies using a combination of socio-economic analysis and time series Landsat TM/ETM+ data over a long time span were relatively scarce. This inevitably limited our understanding of the relationship between human activities and the UHI effect. Thus, the fast-growing Shanghai metropolis in China is taken as an example; the purpose of this study is to utilize an enhanced methodology to address the following questions: (1) How do changes in LULC, urban form, and population shift influence the spatiotemporal patterns of the UHI? (2) What are the relationships between the driving forces and the UHI? and (3) What are the implications for official policies on land use zoning and strategies for mitigating UHI effects and adapting to climate change?

Study area

The study area is the Shanghai metropolitan area, located between latitudes 31°32'N and 31°27'N and longitudes 120°52'E and 121°45'E (Fig. 1). This area has a northern subtropical monsoon climate, with an average annual temperature of approximately 15 °C. The high temperatures average 28 °C in the summer and 4 °C in the winter. The average annual precipitation is approximately 1000–1200 mm, with 60% of the rainfall occurring during May and September. Topographically, the area is primarily located on an alluvial terrace of the Yangtze River basin. The elevation of the area ranges between 1 and 103.4 m, with an average of 4 m.

Administratively, the Shanghai metropolitan area consists of seventeen districts, covering a stable terrestrial area of 6450 km² (excluding recent tidal land reclamation, the Yangtze river estuary waters, and the Hangzhou bay water area), with a total of 18.18 million residents (Shanghai Municipal Statistics Bureau, 2009). This study focuses on the city of Shanghai proper and its surrounding area, which covers an area of approximately 3999.3 km².

To better describe the LULC change patterns, based on our prior knowledge of the land use properties, development intensity, and socio-economic levels of the study area (Li, Zhang, & Kainz, 2012), a total of thirty-two sub-zones was recognized as follows: (1) inner sub-zones within the city proper, enclosed by the inner traffic ring, which are characterized by very dense commercial and residential areas; (2) middle sub-zones at the urban fringe between the inner and outer traffic rings, which are characterized by dense industrial and residential areas; and (3) exurban sub-zones beyond the outer traffic ring, which are characterized by low density to moderate density residential areas, cropland, and natural environment, except for several major industrial parks, such as the Baosteel Corporation in the north and the Wujing chemical industrial park in the south.

Data and methodology

In this study, a working flowchart describing the technical process for the detection of land cover change, the retrieval of land

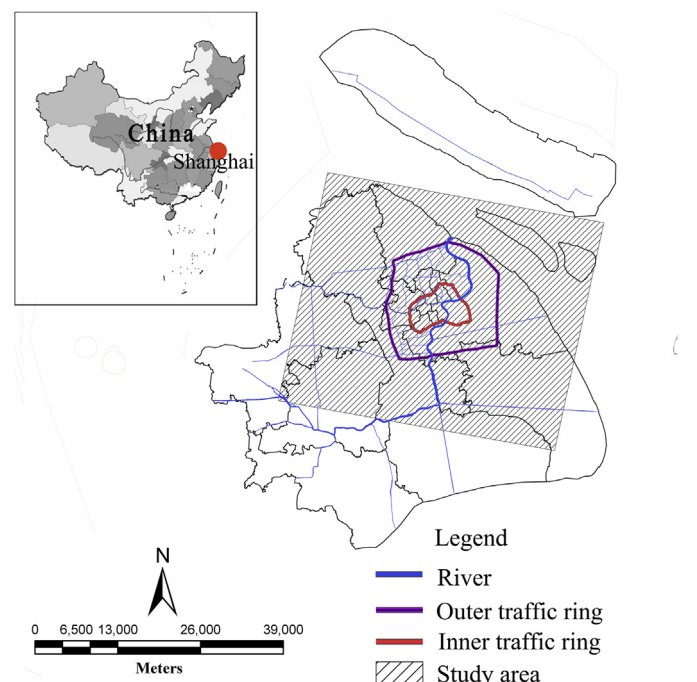


Fig. 1. Location of the study area.

surface temperature (LST), the mapping of LST intensity, and the analysis of the spatiotemporal patterns of LST intensity is shown in Fig. 2.

Imagery preprocessing and classification

To depict the trajectory of urban growth, LULC change, and the spatiotemporal patterns of the UHI, multi-temporal images from Landsat Thematic Mapper (TM) and Landsat Enhanced Thematic Mapper (ETM+) dated April 11, 1997, November 3, 1999, April 27, 2000, July 3, 2001, January 11, 2002, November 27, 2002, December 26, 2003, August 15, 2005, and March 24, 2008, were used in this study. All of the images were clear and nearly free of clouds (total cloud cover less than 10%). The two Landsat ETM+ SLC-off products dated December 26, 2003 and August 15, 2005 were repaired with a self-adaptive local regression model for multi-temporal imagery (Lin & Bao, 2005). As a result, the gap-filled imagery contains most of the available information in comparison with the SLC-on products and thus can be used for further study.

All of the images were rectified and georeferenced to the UTM map projection prior to interpretation. The images were resampled to 30 m. Subsequently, bands 5, 4, and 3 were combined to produce false-color images for visual interpretation. To examine the impacts of human activities on the regional scale, land cover classification was necessary for the detection of LULC change across the study period. Based on our prior knowledge of the land cover from field surveys and previous studies, the classification scheme of the study area was modified in accordance with the land use classification system of the China National Committee of Agricultural Divisions (1984). The major land cover classes used were developed land, cropland, fallow land, forest/shrub, water bodies, and bare land (Table 1).

Supervised signature extraction with a maximum likelihood algorithm was employed to classify the satellite images. For each image, 100 training sites were chosen to ensure that all spectral classes covering each LULC category were adequately represented in the training statistics. The image processing and data manipulation were conducted using algorithms supplied with GEOSTAR 3.0[®]. Furthermore, ESRI ArcGIS 10.1[®] was used for the spatial analyses.

Accuracy assessment and detection of land cover change

Accuracy assessment was performed using the following procedure. First, to increase the accuracy of the land cover mapping of the images, ancillary data, including land use survey data derived from historical aerial photos, four 1:250,000 digitized land use maps from 1993, 1996, 2000, and 2003 and a SPOT image from 2007 from the Shanghai Institute for Geological Survey, were used to collect the reference data. Second, for each classified map, 50 samples for each land use class were selected using a stratified random method to represent the different land cover classes of the study area. Therefore, 300 samples each were used to check the accuracy of the classified maps. Then, the reference data and the results of the visual interpretation were combined with the classification results to improve the classification accuracy of the classified images (Shalaby & Tateishi, 2007). The KAPPA indices for the 1997 and 2008 maps were 86.7% and 88.3%, respectively, which met the recommended value of Jassen, Frans, and Wel (1994), implying that these data were available for further study.

Subsequently, post-classification comparisons were employed to detect LULC change (Singh, 1989). A land use change matrix was produced showing the quantitative data of the overall land use and

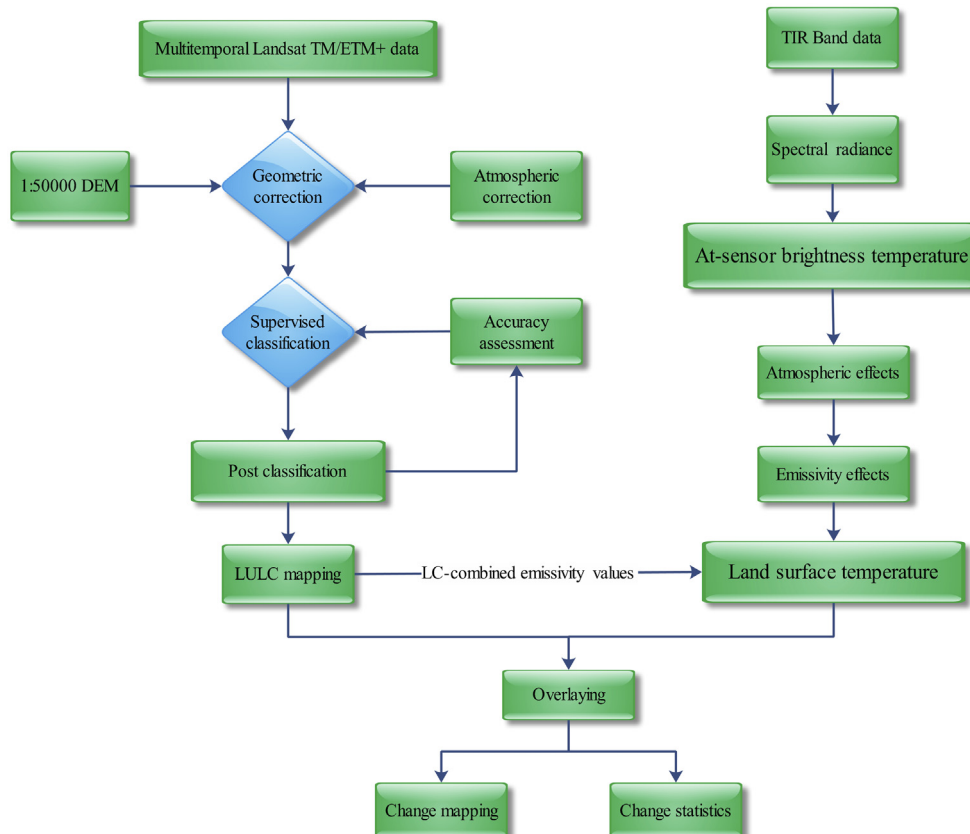


Fig. 2. Working flowchart for this study.

Table 1

Description of land cover types in the study area.

Land cover class	Description
Developed land	Mainly including residences, commercial centers, industrial zones, railways, highways, expressways, docks, and harbors
Farmland	Arable agricultural land, including paddy field, vegetable field, and dry land
Fallow land	Abandoned agricultural land with lower vegetation cover, or temporarily unvegetated land after harvest
Forest and shrub	Mainly including natural and semi-natural forestlands, shrub lands, and forest nursery
Water bodies	Mainly including rivers, creeks, ponds, lakes, reservoirs, permanent and seasonal wetlands
Bare land	Land without vegetation cover, mainly including exposed soil and landfill sites

cover changes between 1997 and 2008 in the study area. Based on the primary types of gains and losses in each category shown in the change matrix, land use transfer images and a land use transfer matrix for each category were also produced.

Retrieval of LST and measurement of UHI intensity

In this study, the image-based method was employed to retrieve LST from Landsat TM/ETM+ data due to its simplicity and validity (Ding & Xu, 2008), compared with the other frequently used algorithms, such as the mono-window algorithm (Qin, Karnieli, & Berliner, 2001) and the single-channel algorithm (Jimenez-Munoz & Sobrino, 2003). However, some uncontrolled and uncertain factors limited the application of this method. For instance, it is very difficult to acquire near-real time atmospheric profile parameters when the satellites pass over the study area throughout the study period. Alternatively, prior to the retrieval of the LST data, a quadratic model was used to convert the digital number (DN) of the Landsat TM thermal TIR band into radiant temperature (Malaret, Bartolucci, Lozano, Anuta, & McGillem, 1985)

$$T_B = 209.831 + 0.834\text{DN} - 0.00133\text{DN}^2 \quad (1)$$

For the Landsat ETM+ thermal TIR band, another model was used, as follows:

$$L_\lambda = \text{gain} \times \text{DN} + \text{offset} \quad (2)$$

where L_λ is the radiance of the thermal band pixels in $\text{W}/(\text{m}^2 \text{ ster } \mu\text{m})$, gain is the slope of the radiance/DN conversion function, and offset is the intercept of the radiance/DN conversion (Landsat Project Science Office, 2002).

Adopting the conversion formula, the spectral radiance was then converted to an at-satellite brightness temperature under the assumption of uniform emissivity (Landsat Project Science Office, 2002).

$$T_B = \frac{K_2}{\ln\left(1 + \frac{K_1}{L_\lambda}\right)} \quad (3)$$

where T_B is the effective at-satellite temperature in K, and both K_1 and K_2 are pre-launch calibration constants ($K_2 = 1282.71 \text{ K}$, $K_1 = 666.09 \text{ mW cm}^{-2} \text{ sr}^{-1} \mu\text{m}^{-1}$).

According to Equation (3), the temperature values obtained above were referenced to a black body, which is quite different from the properties of real objects. Therefore, correction of the spectral emissivities (ϵ) was performed considering the natures of the land cover types. It is very difficult to obtain emissivities directly for Landsat TM/ETM+ data, given there is only a single window for TIR

data (Li, Jackson et al., 2004; Li, Zhang et al., 2004). The emissivities for the land cover types based on empirical models are widely used. In this study, the estimated emissivities for the vegetated areas, developed areas, bare land, and water bodies were 0.95, 0.923, 0.92, and 0.9925, respectively (Artis & Carnahan, 1982; Nichol, 1996). Furthermore, the emissivity-corrected land surface temperature was computed as follows (Artis & Carnahan, 1982):

$$T_s = \frac{T_B}{1 + (\lambda \times T_B/\alpha)\ln\epsilon} \quad (4)$$

where T_s is the surface radiant temperature in Kelvin (K), T_B the black body temperature in Kelvin (K), λ is the wavelength of emitted radiance, herein, $\lambda = 11.5 \mu\text{m}$ (Markham & Barker, 1985), and $\alpha = hc/K$ ($1.438 \times 10^{-2} \text{ mK}$), where h is Planck's constant ($6.626 \times 10^{-34} \text{ J s}^{-1}$), c is the velocity of light ($2.998 \times 108 \text{ m s}^{-1}$), K is Boltzmann's constant ($1.38 \times 10^{-23} \text{ J K}^{-1}$), and ϵ is the surface emissivity.

Subsequently, combined with land cover maps, the average LST for each land cover type was computed. The UHI intensity can be indicated by the difference in LST between urban and surrounding areas (Hung, Uchihama, Ochi, & Yasuoka, 2006; Pongrácz et al., 2010). Thus, in this study, two UHI intensity indices were defined: one is the UHI intensity between the city proper and the surrounding rural area (ΔT_{C-R}), and the other is the UHI intensity between the urban fringe and the surrounding rural area (ΔT_{P-R}). Subsequently, based on our overall understanding of the spatio-temporal pattern of UHIs, the UHI intensity levels were divided into six levels as follows:

- Level I: Very low, meaning the LST difference between the urban and surrounding areas is equal to or less than zero;
- Level II: Slightly low, meaning the LST difference between the urban and surrounding areas is between 0 and 1 °C;
- Level III: Low, meaning the LST difference between the urban and surrounding areas is between 1 and 2 °C;
- Level IV: Medium, meaning the LST difference between the urban and surrounding areas is between 2 and 3 °C;
- Level V: High, meaning the LST difference between the urban and surrounding areas is between 3 and 4 °C;
- Level VI: Very high, meaning the LST difference between the urban and surrounding areas is over 4 °C.

Estimation of the sub-zonal population density

In this study, the population density of each district was extracted from the statistical yearbook of Shanghai (Shanghai Municipal Statistics Bureau, 2009). As shown in Fig. 1, according to our pre-defined spatial extent, based on the inner and outer traffic rings, some districts were divided into two or three neighboring sub-zones. Because there were no available estimates of population density for these sub-zones, we readjusted the distribution pattern of the population of each sub-zone, with the assumption that the population resided on the developed land. Thus, the ratio of the sub-zonal PDL to the total PDL within the administrative boundary of each district was used as the weight factor, which was then multiplied by the district-based population density and the monthly mean population growth rate for each year to generate the estimated population density of these sub-zones. The estimated sub-zonal population density was calculated as follows:

$$\text{Pop_density} = \frac{\text{District Pop} \times (1 + \text{MMGR})^n \times A_1/A_2}{A_3} \quad (5)$$

where Pop_density is the sub-zonal population density (1000 persons per km²), District Pop is the population size within the administrative boundary of each district, MMGR is the monthly mean growth rate of the population within each district, *n* is the number of months between the acquisition dates for two neighboring satellite images, *A*₁ is the sub-zonal percentage of developed land (PDL), and *A*₂ is the total PDL within the administrative boundary of each district. Both *A*₁ and *A*₂ were measured using the spatial analyst embedded in ArcGIS 10.1. *A*₃ is the areal extent of each sub-zone.

Statistical analysis

Quantitatively examining the relationship between LST and the related driving forces is necessary to understand the processes and mechanisms of the UHI effect associated with human activities. Sub-zonal variables, including mean LST, mean percentage of water bodies (PW), mean percentage of vegetated land (PV), mean percentage of developed land (PDL), and mean population density (Pop_den) were generated for the defined extent of the thirty-two sub-zones. Similar to the aforementioned computation of PDL, mean LST, PW, and PV were computed using the spatial analyst embedded in ArcGIS 10.1. In the subsequent statistical analysis, descriptive statistics and scatter plots were completed prior to choosing the appropriate statistical procedures for the variables. Accordingly, a non-linear regression model was employed to examine the relationship between the annual mean population density and the annual mean growth rate of developed land, by carefully checking the significance tests for the overall distributions and the interactive function relationships of the variables. A Kruskal–Wallis test was employed to test whether there was a significant difference in mean UHI intensity across all seasons, given that not all of the grouped data met the requirement of equal variance. Furthermore, to examine the relationship between mean LST and

three independent variables (PW, PV, and PDL), analyses of Pearson's product–moment correlation and linear regressions were performed. Unfortunately, both the results of the Pearson's product–moment correlation for independent variables and the linear regression between the dependent and independent variables exhibited high statistical significance (*p* < 0.05), indicating that there was strong collinearity between the dependent and independent variables. Obviously, a multiple regression model is not applicable. Alternatively, to remove the collinearity, we adopted partial least squares regression (PLS) models exploring the relationships between LST and the related driving factors (see Equation (6)).

$$\text{LST} = \alpha + \beta_1 \cdot \text{PW} + \beta_2 \cdot \text{PV} + \beta_3 \cdot \text{PDL} + \varepsilon \quad (6)$$

where α is a constant, β_1 , β_2 , and β_3 are the associated coefficients of the regressive items, and ε is the random error term.

Moreover, the leave-one-out cross-validation method was used to select the optimal number of PLS factors included in the regression models (Geladi & Kowalski, 1986). Both the coefficient of determination (R^2) and the *p* value (0.05) were used to validate the performance of the PLS regression model.

These statistical processes were performed using the commercial data processing system (DPS[©]12.5) statistical package (Tang, 2010, p. 1140).

Results

Land use dynamics and developed land expansion

Generally, Figs. 3 and 4 show the land use dynamics of the city of Shanghai across the study period, at nearly even two-year intervals. As shown, the spatial extents of the land cover types and the developed land expansion rates varied significantly over different periods.

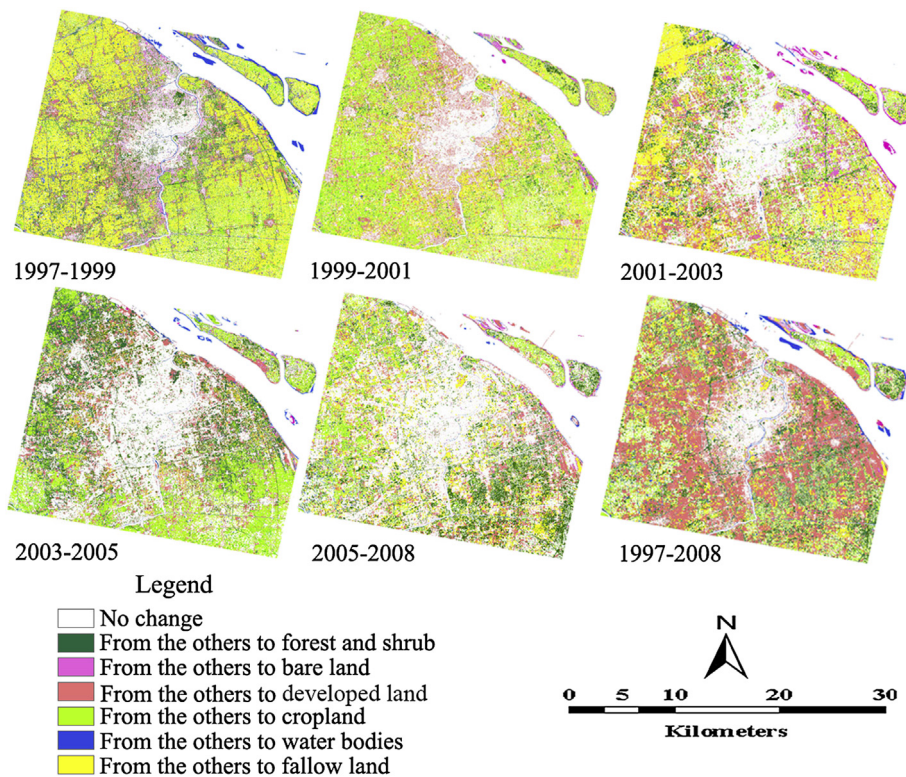


Fig. 3. LULC change maps of the study area for 1997 and 2008.

In the period 1997–1999, the area of developed land increased by 23390.73 ha. The expansion of developed land primarily occurred within the middle sub-zones of the urban fringe, between the inner and outer traffic rings. Fallow land in this domain was the major contributor (20.97%) to the newly emerging developed land, followed by forest and shrub (11.97%), bare land (9.74%), and cropland (6.45%).

In the period 1999–2001, the developed land area increased by 32973.39 ha. Forest and shrub was the major contributor (16.05%) to the newly emerging developed land, followed by cropland (10.87%), bare land (7.42%), and fallow land (5.47%).

In the period 2001–2003, the developed land area increased by 38689.74 ha. As the major contributors, fallow land and cropland accounted for 16.76% and 15.06%, respectively, of the newly emerging developed land.

In the period 2003–2005, the developed land area increased by 16473.69 ha. As the major contributors, fallow land and cropland accounted for 10.71% and 9.14%, respectively, of the newly emerging developed land.

In the period 2005–2008 the developed land area increased by 6228.27 ha. Forest and shrub and cropland became the major contributors, accounting for 10.77% and 7.96%, respectively, of the newly emerging developed land.

Overall, in the period 1997–2008, the developed land area increased by 219.50%. Approximately 72.52% of the newly emerging developed land was converted from former cropland (24.79%), fallow land (21.21%), forest and shrub (18.97%), bare land (6.62%), and water (0.93%). The net increase in developed land is clearly at the expense of the aforementioned land uses.

Analysis of population shift and developed land dynamics

Fig. 5 shows the relationships between the annual mean percentage of developed land and the population density for each sub-zone for 1997 and 2008. As shown, there were remarkably different patterns for the annual mean population density and percentage of developed land within these sub-zones. For the inner sub-zones, the annual mean percentage of developed land increased from 87.65% in 1997 to 90.57% in 2008. Meanwhile, the annual mean population density decreased from 31,053 persons/km² in 1997 to 26,239 persons/km² in 2008. There was a significant negative relationship between the annual mean population growth and the expansion of developed land in the inner sub-zones. For the middle sub-zones, a remarkable increase in the annual mean percentage of developed land was observed, but the trend in the annual mean population growth was relatively stable. Not surprisingly, there was

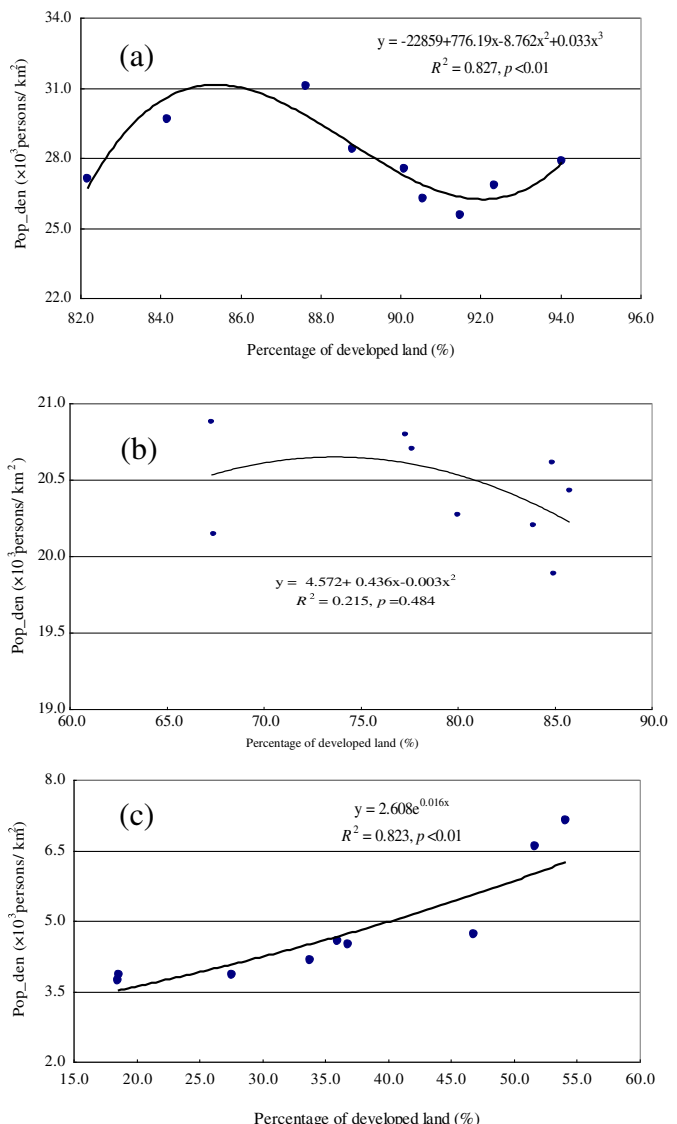


Fig. 5. Relationship between the percentage of developed land and the population density within different sub-zones (standard errors of the two variables are shown). Note: **Fig. 5a** shows the sub-zones within the city proper enclosed by the inner traffic ring; **Fig. 5b** shows the middle sub-zones at the urban fringe between the inner and outer traffic rings; and **Fig. 5c** shows the exurban sub-zones beyond the outer traffic ring.

no statistically significant relationship between them. In contrast, for the exurban sub-zones, the estimated annual mean percentage of developed land increased from 18.59% in 1997 to 54.12% in 2008, accompanied by synchronous population growth, as shown by the increase in annual mean population density from 3851 persons/km² to 7126 persons/km² over the same time.

In addition, **Table 2** shows the trends in the annual mean growth rates of developed land and the population shift, both with marked variation during the different time periods. For the inner sub-zones, the higher growth rate of developed land for 1999–2001 offset those of the other time periods with negative values. Meanwhile, the ongoing decline in the population growth rate dominated across all time periods except 2005–2008. As a result, the cumulative change in population growth rate (−7.76%) was much significant than that of developed land (1.66%), implying the net emigration of the population. For the middle sub-zones at the urban fringe, between the inner and outer traffic rings, similar trends in annual

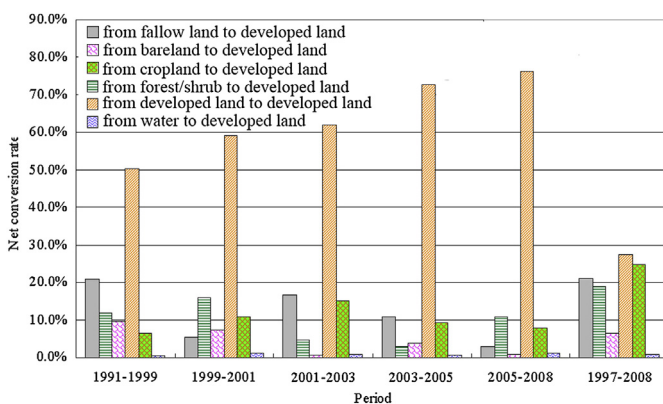


Fig. 4. Variation in rates of net conversion of the other land cover types to developed land.

Table 2

Trends in annual mean growth rates of developed land area and population size.

Stage	Spatial extent of sub-zones		
	Inner	Middle	Exurban
1997–1999	−1.98% (−2.25%)	0.33% (−2.00%)	27.14% (−2.24%)
1999–2001	5.86% (−3.01%)	12.56% (−0.10%)	43.70% (3.74%)
2001–2003	−0.90% (−1.88%)	0.81% (−0.83%)	21.67% (6.22%)
2003–2005	−0.47% (−2.42%)	0.60% (1.09%)	5.80% (23.64%)
2005–2008	−0.34% (0.93%)	−2.26% (−0.14%)	1.91% (3.67%)

Note: 'Inner' denotes the sub-zones within the city proper enclosed by the inner traffic ring; 'Middle' denotes the middle sub-zones at the urban fringe between the inner and outer traffic rings; 'Exurban' denotes the exurban sub-zones beyond the outer traffic ring; annual population growth rate is in parenthesis.

mean growth rates of developed land area and population size were observed. The cumulative change in population growth rate (−2.06%) during the period 1997–2008 can be attributed to the expansion of developed land, as evidenced by the cumulative growth rate of developed land (10.38%). In contrast, increasing trends in the growth rates of both developed land area and population size were observed within the exurban sub-zones beyond the outer traffic ring. Obviously, both cumulative changes in developed land area and population size within the exurban sub-zones were much higher than the inner sub-district units and middle sub-zones at the urban fringe. Therefore, variations in the annual mean and cumulative growth rates of both developed land area and population size exhibited an urban–suburban–exurban gradient in the population shift during the period 1997–2008, as evidenced by the remarkably increasing annual mean and cumulative growth rates of developed land. In addition, as shown in the land use patterns in Fig. 3, the newly emerging settlements and booming industrial parks that developed in the urban fringe and exurban area may help explain the population shift trends associated with the dynamics of developed land across the aforementioned three sub-zone levels. A detailed cause-effect analysis of developed land expansion and population shift and their influence on the spatiotemporal patterns of UHIs will be presented in the Discussion section.

Spatiotemporal patterns of UHI intensity

Visually, Fig. 6 shows the spatiotemporal patterns of UHI intensity (ΔT) for 1997–2008. Apparently, there was remarkable seasonal and inter-annual variation in UHI intensity among the land cover types (see Fig. 7a–h). In addition, as observed from Fig. 8, an overall trend in UHI intensity meant that both the summertime means of ΔT_{C-R} and ΔT_{P-R} had the maximum values, followed by the springtime means of ΔT_{C-R} and ΔT_{P-R} with significant temporal variation. In contrast, both the autumntime and wintertime means of ΔT_{C-R} and ΔT_{P-R} were much lower. In addition, the springtime mean ΔT_{C-P} had the maximum value, followed by the summertime mean ΔT_{C-P} and the autumntime mean ΔT_{C-P} , whereas the wintertime mean ΔT_{C-P} had the minimum value. However, the results of the Kruskal–Wallis test show that, in general, there were no significant differences among the mean ΔT_{C-P} values across all seasons ($df = 3, H = 5.11, P = 0.164$), indicating that the rapid outward expansion of the developed area has led to increasing mean LSTs in the urban fringe.

Furthermore, Fig. 9a–d shows the distribution of the UHI intensity levels across the study period. As shown, both the magnitude and intensity of the UHI varied remarkably, depending on the changes in the different years, seasons, and accompanying land cover types. On average, in percentage terms, the background UHI intensity ranked level I (very low) accounted for 47.14–53.32% across all seasons due to the existence of a large percentage of

cooler surfaces, such as water bodies and vegetated surfaces. Therefore, except for the background UHI intensity level, the percentages of the other UHI intensity levels, ranging from II (slightly low) to VI (very high), exhibited a relatively even pattern in the spring, although the percentages of levels V (high) and VI (very high) were the highest (18.27%) across all of the seasons. In summer, the percentages of the low and medium UHI intensity levels slightly surpassed the high and very high levels (11.16%). In autumn and winter, an uneven distribution pattern for the UHI intensity levels was observed, as evidenced by the much higher percentages of slightly low level (41.45% in autumn and 26.37% in winter) and low level UHI intensity (10.16% in autumn and 23.01% in winter). In contrast, the percentages of the high and very high levels accounted for 0.27% in autumn and 0.14% in winter.

Drivers of UHI intensity

Table 3 shows the significant linear relationship between UHI intensity and the underlying driving factors. As shown, the partial coefficients of the independent variables for LST and UHI intensity fluctuated markedly due to the annual and seasonal variation in land cover and human activities, but other factors, such as regional weather conditions and land surface biophysical features, may contribute to the significant variation in UHI intensity, although these vital factors were not included in our model due to the unavailability of the data at the sub-zone and regional scales. However, overall, across the study period, PW and PV are generally the dominant factors in determining the UHI intensity levels, except during two summertime events (dated July 3, 2001 and August 15, 2005), followed by PDL and Pop_den, when the effects of the other factors are kept constant. In addition, from the mean partial coefficients of the independent variables, the coefficients of PW and PV had higher values during spring and summer but lower values during autumn and winter. This trend is consistent with the data shown in Fig. 7 and indicated that the land cover types dominated by water bodies and vegetation, especially the rural area beyond the outer traffic ring, exhibited lower mean LST than did the urban agglomeration and the aggregated developed land, where impervious surfaces and sparsely vegetated land dominate the land cover types.

Discussion

In the context of anthropogenic climate change and global warming, understanding and active management of LULC change is increasingly important (Turner, Lambin, & Reenberg, 2007). As presented in previous studies, the occurrence of UHIs depends on many factors, including the large-scale and meso-scale climatic conditions, microclimate, geographical location, biophysical features of the land surface, urban structure, population size, wind corridor, human lifestyle, and energy consumption (Oke, 1982; Taha, 1997). Given the diversity and complexity of these natural and artificial processes, the underlying causes and effects of UHIs, full consideration of incorporating these processes into a broader background of demographic, economic and social transformations is required (Dodman, 2009). Thus, in this section, the focus is on LULC change, developed land expansion, and UHI effects, and their implications for sustainable urban planning and adaptation to climate change are discussed.

Official land use zoning policy and its influence on LULC change and population shift

Since the 1990s, the Shanghai metropolitan area has experienced an unprecedented socio-economic transition. According to

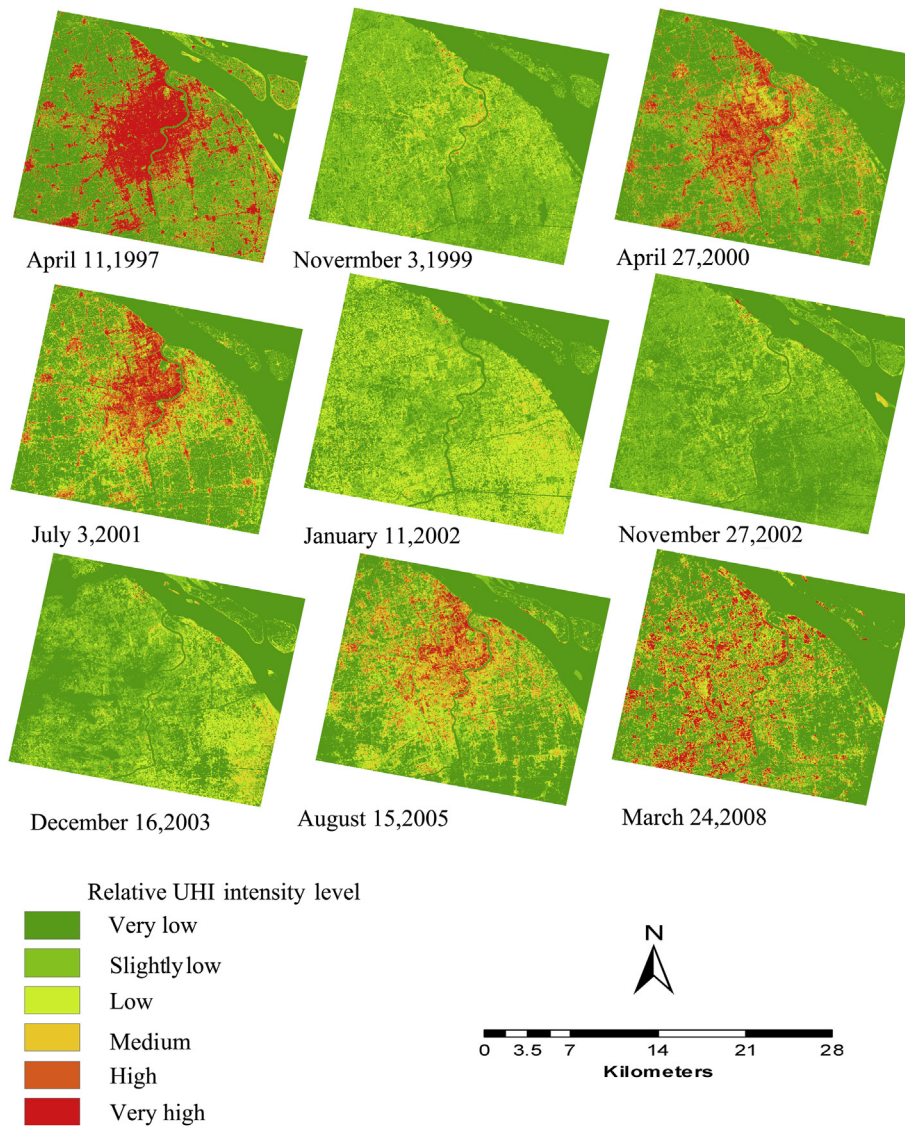


Fig. 6. UHI intensity levels retrieved from the multi-temporal Landsat TM/ETM+ data.

the national strategy known as 'opening the Pudong New Area to the world', the role of this city in the 21st century was to be a globally leading mega city, with international centers for finance, trade, shipping, and information technology businesses in the Asia-Pacific region (Shanghai Municipal Government, 2000). To achieve the goals of upgrading the industrial levels and coordinating urban–suburban development, the functions of the city proper were oriented as an urban agglomeration for commerce, modern services, administrative land, and settlement, whereas the functions of the urban fringe and exurban area were oriented as the receptors for industry transfer and the key manufacturing base, especially for the automobile manufacturing, the information technology (IT), the precision instruments, and the biopharmaceutical industries and entire sectors of the equipment manufacturing industry (Shanghai Municipal Commission of Economy and Information, 2008).

Facing the challenges of land use change under a market economy and a public increasingly concerned for the urban environment as well as quality of life, the municipal government and district governments have taken great efforts to propel urban regeneration, decentralize the dense population, optimize the economic structure, and adjust the industrial layout. Over the past

decade, many traditional industrial polluters within the city proper have closed or relocated to suburban and exurban industrial parks. Simultaneously, numerous old residences in the city proper have been demolished, and 900,000 residents were resettled into the urban fringe and surrounding satellite towns (Li & Nin, 2007) due to the successful implementation of government-oriented urban renewal policies.

In contrast, the urban fringe and exurban areas have been the preferred destinations for numerous domestic and international enterprises, given the location advantage, lower land prices, newly emerging competitive industrial clusters, impeccable municipal facilities, official policies favoring the attraction of capital, and the social services network. Most of the intensive industrial parks were established in the urban fringe and exurban areas, where there are existing industrial clusters, especially in the neighborhood near the outer traffic ring and exurban satellite towns, such as Wusong, Yuepu, Nanxiang, Taopu, Gaoqiao, Jinqiao, Zhangjiang, Beicai, Anting, Xinzhuang, and Wujing, where both traditional and advanced manufacturing industries have enjoyed a boom. Nevertheless, the government-oriented policies of industrial restructuring and the relocation of colleges have changed both the direction

of the rural–urban population shift and the flow of capital investment. For instance, to meet the challenges of economic globalization and the knowledge economy, to attract domestic and international competitive enterprises, and to accelerate

intelligence-based industrial clusters, which desirably require creative researchers, qualified engineers, and skilled workers, the municipal government issued an official executive order to guide the relocation of universities and colleges to the urban fringe.

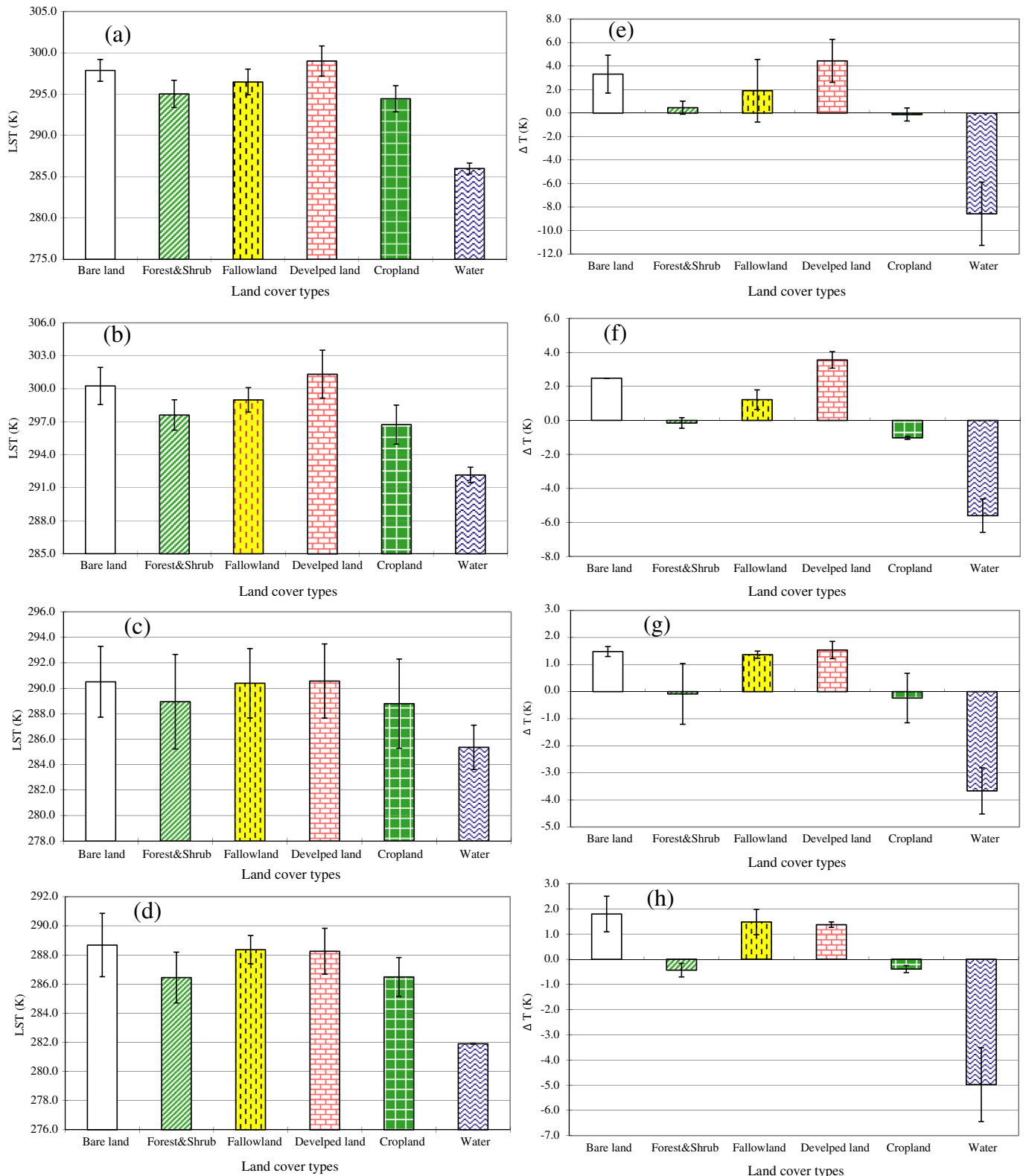


Fig. 7. Inter-annual and seasonal variation in the average LST of each land cover type (shown in Fig. 7a-d) and the average LST differences (ΔT) between each land cover type and the surrounding landscape (shown in Fig. 7e-h). a and b Average LST of each land cover type in Spring and Summer. c and d Average LST of each land cover type in Autumn and Winter. e and f Average ΔT of each land cover type in Spring and Summer. g and h Average ΔT of each land cover type in Autumn and Winter.

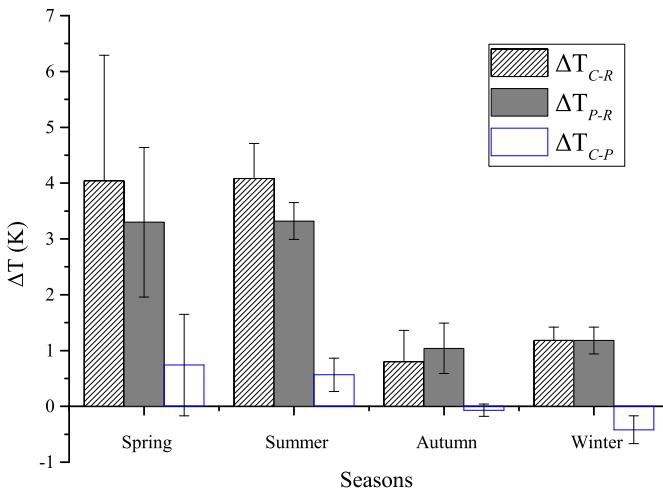


Fig. 8. Seasonal variation in the mean UHI intensity of the study area. Note: ΔT_{C-R} is the LST difference between the city proper and surrounding rural areas, ΔT_{P-R} is the LST difference between the urban fringe and the surrounding rural areas, and ΔT_{U-P} is the LST difference between the city proper and the urban fringe.

Accordingly, suburban district governments enacted favorable policies and competitive strategies to attract the universities and colleges. Thereafter, several universities and colleges, including Shanghai Jiaotong University, East China Normal University, and the Shanghai Foreign Trade College, moved to intensive college parks neighboring the major industrial parks in Minhang district and Songjiang district. The other two examples are the Zhangjiang high-tech park at the Pudong New Area and the Anting automobile city in Jiading district. In Zhangjiang high-tech park, the IT trade and biomedical industry are the dominant industries. The Software School of Fudan University and the entirety of the Chinese Medicine University have relocated there. The Anting automobile city is jointly propelled by the Volkswagen Group and its local strategic partner, the Automobile Engineering School of Tongji University. These actions have not only led to population shifts from the populated city proper to the urban fringe and exurban satellite towns but also have attracted millions of inter-provincial migrants.

LULC change, population shift and their influence on patterns of UHI intensity

As mentioned above, official land use zoning policies resulted in the urban–suburban–exurban gradient patterns in the population shift, made evident by a sharp increase in developed land within the middle sub-zones at the urban fringe and the exurban sub-zones beyond the outer traffic ring. According to the implemented urban planning, the replaced lands within the city proper were largely used for higher-value land, such as commercial facilities and real estate, with only a small percentage used for municipal reconstruction and green space. These actions consequently stimulated the booming development of the central business districts (CBD) and the modern residential quarters, which inevitably increased the impervious surface cover with its high-heat capacity (Dai, Guo, Zhang, & Li, 2010). Meanwhile, because of the rapid development and resultant population agglomeration in the middle sub-zones at the urban fringe and the exurban sub-zones beyond the outer traffic ring, there was a strong demand for land development. As addressed in our earlier study (Li et al., 2012; Zhang, Zhou, Chen, & Ma, 2011), the outward expansion of the developed land implied that the local authorities took no action to slow this urbanization process. To improve the infrastructure and

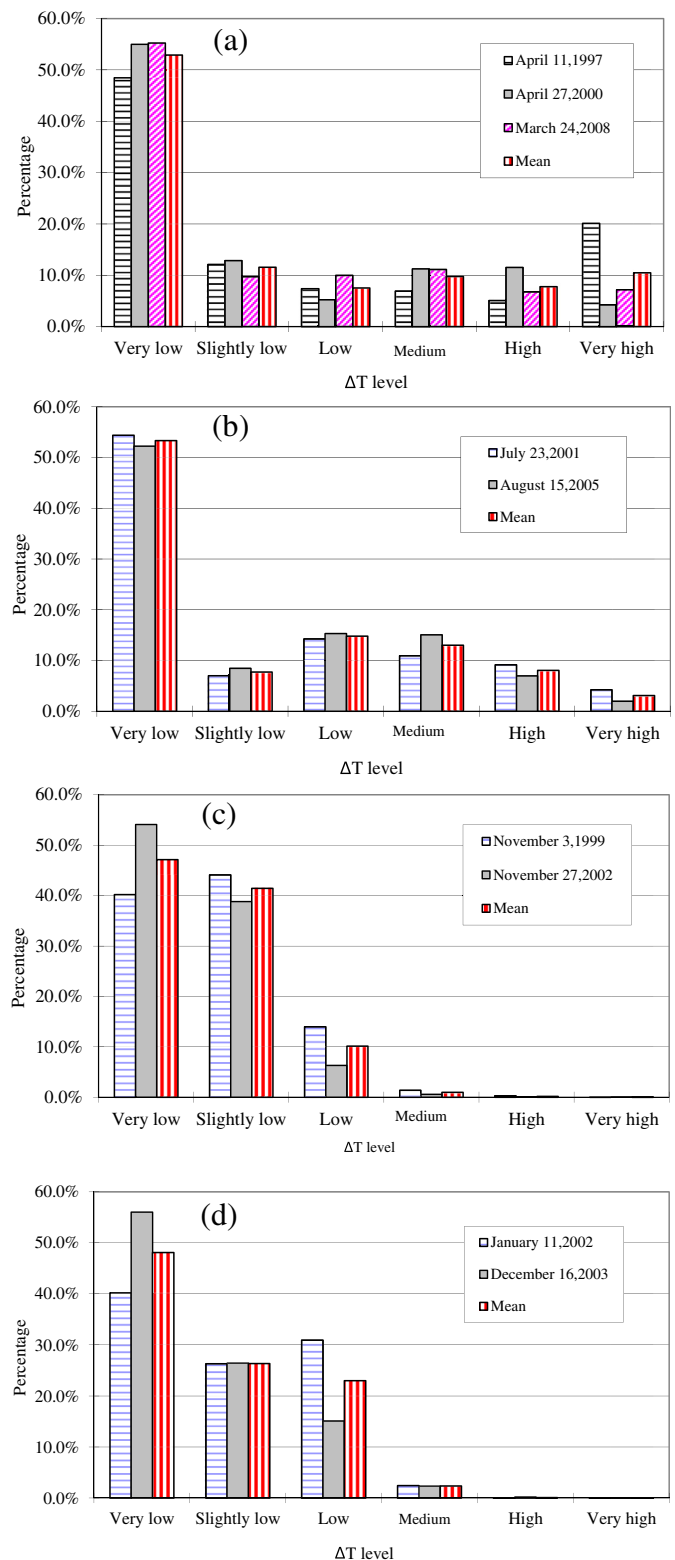


Fig. 9. Distribution of the UHI intensity levels across the study period. a and b UHI intensity levels in Spring and Summer. c and d UHI intensity levels in Autumn and Winter. Note: Fig. 9a–d denotes the distribution of the UHI intensity levels in the springtime, summertime, autumntime, and wintertime, respectively.

service capacities, to accommodate the increasing population, and to create more employment opportunities, a series of key projects, such as inter-provincial highways, expressways, intensive settlements, and industrial facilities, have been invested in and well

Table 3PLS regression equations for UHI intensity (ΔT) and related driving factors.

Season	Acquisition date (YY/MM/DD)	Fitted regression equation	R^2	p
Spring	1997/04/11	$\Delta T = 5.551 - 0.098PW - 0.060PV + 0.018PDL + 0.004Pop_den$	0.975	0.000
	2000/04/27	$\Delta T = 4.330 - 0.041PW - 0.060PV + 0.001PDL + 0.005Pop_den$	0.950	0.000
	2008/03/24	$\Delta T = 1.920 - 0.061PW - 0.017PV + 0.008PDL + 0.002Pop_den$	0.387	0.016
	Mean	$\Delta T = 4.178 - 0.081PW - 0.048PV + 0.006PDL + 0.006Pop_den$	0.937	0.000
Summer	2001/07/03	$\Delta T = 1.113 - 0.068PW - 0.019PV + 0.034PDL + 0.007Pop_den$	0.968	0.000
	2005/08/15	$\Delta T = 0.700 - 0.052PW - 0.019PV + 0.029PDL + 0.016Pop_den$	0.896	0.000
	Mean	$\Delta T = 2.673 - 0.085PW - 0.042PV + 0.014PDL + 0.012Pop_den$	0.958	0.000
Autumn	1999/11/03	$\Delta T = 1.035 - 0.027PW - 0.006PV + 0.009PDL + 0.002Pop_den$	0.659	0.000
	2002/11/27	$\Delta T = 0.620 - 0.023PW - 0.017PV + 0.006PDL + 0.003Pop_den$	0.485	0.002
	Mean	$\Delta T = 0.159 - 0.023PW - 0.002PV + 0.006PDL + 0.002Pop_den$	0.438	0.003
Winter	2002/01/11	$\Delta T = 2.110 - 0.077PW - 0.005PV + 0.002PDL + 0.004Pop_den$	0.690	0.000
	2003/12/16	$\Delta T = 1.220 - 0.053PW - 0.012PV + 0.019PDL + 0.007Pop_den$	0.477	0.007
	Mean	$\Delta T = 2.201 - 0.051PW - 0.059PV + 0.009PDL + 0.002Pop_den$	0.489	0.001

Note: PW, PV, and PDL denote percentages of water bodies, vegetated land, and developed land of each sub-zone, respectively; Pop_den denotes population density (1000 persons/km²).

developed in these hotspots of development. As shown in Fig. 3 and Table 2, the extent of developed land in 1997 was mainly constrained to the compact downtown, and there was a larger proportion of natural and semi-natural surfaces with their cooling effects. Thus, compared with the other UHI intensity areas detected in different years and seasons, the image from April 1997 showed large areas of high UHI intensity. However, since 2001, a remarkable in-filling development pattern occurred along the outer traffic ring and the expressway across the urban fringe and the exurban areas. This has led to urban sprawl along multiple axes, as witnessed by the expansion of developed land, the anthropogenic alteration of land cover, including the replacement of vegetated land with impervious surfaces, the filling of small water bodies for buildings, and the demolishing of rural villages to develop industrial parks. These have resulted in considerable changes in the surface energy balance and heat flux, in particular increased sensible heat flux due to the loss of water bodies and vegetated surfaces. Consequently, the LST difference between the city proper and the urban fringe has been less than before.

Implications for the official strategy toward mitigating UHI effects and adapting to climate change

For all of the stakeholders, it is critical to better understand the mechanisms and impacts of UHIs brought on by the dramatic LULC change and rapid urbanization. Until the present, discussions of the mechanisms and effects of UHIs, such as energy consumption, air pollution, health risks, and mitigation strategies, have been constrained to scholarly research (Tan, 1994) and are therefore far from being adopted into the official decision-making process. Furthermore, in Shanghai and the other domestic cities in mainland China, there are not yet any official executive orders, specific policies, or explicit regulations for mitigating UHI effects and adapting to climate change. As embodied in the strategies of local authorities for adapting to climate change (Shanghai Municipal Government, 2012), the goals of the municipal government are too wide, roughly focusing on reducing energy consumption, curtailing greenhouse gas (GHG) emissions, promoting green building, developing green space, and reinforcing environmental governance. It is unfortunate that the role of UHI effects in regional and local climate change has been neglected. Nevertheless, this city has lagged behind its international counterparts such as New York, Houston (Hitchcock, 2006), New Jersey (Soleckia et al., 2005), Toronto (Akbari & Konopacki, 2004), Tokyo, Osaka, and Fukuoka (Yamamoto, 2006), which have explicit strategies for mitigating UHI effects and adapting to climate change. The implementation of policies based on sound understanding of LULC change, urban

structural evolution, population shifts, anthropogenic heating, building materials, tree cover, and their influences on UHI effects is indispensable. Increasing green space is officially regarded as an appropriate and practical approach to abate UHI effects. To achieve the goal of a better urban quality of life, the Shanghai municipal government and the subordinate district governments have generously invested in urban green spaces. These actions included cultivating urban forests along the outer traffic ring, planting and conserving green corridors along the major rivers, and developing small patches of green space within a 500-m radius of major residences. Urban green space has increased by 336.44%, from 7849.0 ha in 1997 to 34256.0 ha in 2008 (Shanghai Municipal Statistics Bureau, 2009). In response, recent studies have shown that emerging green spaces have helped to partially decrease UHI effects within the urbanized area on warmer and hot days, especially in the populated city proper (Ding, Zhou, & Ye, 2002; Ge, Zhou, & Tu, 2005). Unfortunately, due to very scarce land resource and strong competition for land development, it is very difficult to merely increase green spaces in the aforementioned hotspots to offset the UHI effects of extreme weather events. Thus, it is urgent that local authorities prudently rethink their policies and enact explicit strategies for mitigating UHI effects and adapting to the new challenge of climate change.

Limitations of this study

By using multi-temporal remotely sensed data and statistical analysis, our study presented better results for the spatiotemporal patterns of the UHI effect and the underlying driving factors than have previous studies using fewer remotely sensed data points or focusing on the relatively smaller area of the Shanghai downtown or through the outer traffic ring. However, several inherent factors have inevitably biased the spatiotemporal patterns of the UHI in this study. First, we used only Landsat TM/ETM+ TIR data to retrieve the patterns of the daytime UHI; thus, the satellite overpass time was not synchronous with that of the sparsely distributed meteorological stations. Second, more attention should be paid to the nighttime UHI pattern because nocturnal UHI intensity might be more pronounced. Thus, in future research, synchronous data from in-situ observations should be combined with multi-temporal, long time span satellite data to produce more accurate results.

Conclusions

Using the fast-growing Shanghai metropolitan area as an example, this paper quantitatively examined the relationships

between land use, developed land expansion, and population shift and their influence on spatiotemporal patterns of urban heat islands using time series Landsat TM/ETM+ imagery and demographic data from 1997 and 2008. Over the studied period, the Shanghai metropolis has undergone dramatic changes in LULC, as evidenced by a sharp increase in developed land, which caused loss of cropland, fallow land, forest and shrub. The developed land increased by 219.50%, approximately 72.52% of which was converted from former cropland (24.79%), fallow land (21.21%), forest and shrub (18.97%), bare land (6.62%), and water (0.93%). Furthermore, in combination with the detection of LULC change, an analysis of the spatially differential growth rates of developed land area and population size revealed the urban–suburban–exurban gradient pattern for the population shift, as evidenced by a sharp increase in developed land within the middle sub-zones at the urban fringe and in the exurban sub-zones beyond the outer traffic ring. Consequently, changes in LULC, developed land expansion, and population shifts resulted in significant variation in the spatiotemporal patterns of UHIs. As revealed, land cover types dominated by water bodies and vegetation, especially rural areas beyond the outer traffic ring, exhibited lower mean LST than did urban agglomeration and aggregated developed land, within which impervious surfaces and sparsely vegetated land dominate the land cover types. The rapid outward expansion of the extent of the developed area has led to considerable changes in the surface energy balance and heat flux, in particular increasing the sensible heat flux due to the loss of water bodies and vegetated surfaces, and thus, the LST difference between the city proper and the urban fringe is less than before.

Moreover, based on a deeper understanding of the results, the relationships between the LULC change, UHI effect, and regional climate change require that the underlying mechanisms, patterns, and processes of land conversion as well as the response of urban climate should be addressed throughout official decision-making processes. Thus, the planners and decision-makers could fully evaluate the environmental consequences of different land development scenarios and therefore have scientific basis with which to improve future planning and regulations, with the objective of mitigating the adverse effects of the UHI and enforcing the adaptation capacity of human-dominated ecosystems.

Acknowledgments

This study was supported by Natural Scientific Foundation of Shanghai (Grant No. 11ZR1401900), Natural Scientific Foundation of China (Grant Nos. 41171432 and 71173049). We would like to thank the International Scientific Data Service Platform operated by Computer Network Information Center, Chinese Academy of Sciences, who generously provide online technical service for repairing Landsat ETM + SLC-off products. Also, special thanks to Center for Earth Observation and Digital Earth, Chinese Academy of Sciences, who kindly provide available Landsat TM/ETM+ imagery within the framework of sharing program for earth observation data. In addition, the authors are indebted to three anonymous reviewers and the editors who help us improve the quality of this manuscript.

References

- Akbari, H., & Konopacki, S. (2004). Energy effects of heat-island reduction strategies in Toronto, Canada. *Energy*, 29, 191–210.
- Aniello, C., Morgan, K., Busbey, A., & Newland, L. (1995). Mapping micro-urban heat islands using LANDSAT TM and a GIS. *Computers and Geosciences*, 21(8), 965–969.
- Artis, D. A., & Carnahan, W. H. (1982). Survey of emissivity variability in thermography of urban areas. *Remote Sensing of Environment*, 12, 313–329.
- Chen, X.-L., Zhao, H.-M., Li, P.-X., & Yin, Z.-Y. (2006). Remote sensing image-based analysis of the relationship between urban heat island and land use/cover changes. *Remote Sensing of Environment*, 104(2), 133–146.
- Dai, X., Guo, Z., Zhang, L., & Li, D. (2010). Spatio-temporal exploratory analysis of urban surface temperature field in Shanghai, China. *Stochastic Environmental Research and Risk Assessment*, 24, 247–257.
- Ding, F., & Xu, H.-Q. (2008). Comparison of three algorithms for retrieving land surface temperature from Landsat TM thermal infrared band. *Journal of Fujian Normal University (Natural Science Edition)*, 24(1), 91–96 (in Chinese).
- Ding, J.-C., Zhou, H.-M., & Ye, Q.-X. (2002). Importance of city green by investigation on evolution of heat island in Shanghai City. *Meteorological Monthly*, 28(2), 22–24 (in Chinese).
- Dodman, D. (April 2, 2009). United Nations Population Fund (UNFPA) analytical review of the interaction between urban growth trends and environmental changes : Paper 1 urban density and climate change (Revised Draft). <http://unfpa.org/webdav/site/global/users/schensul/public/CCPD/papers/Dodman%20Paper.pdf>
- Dousset, B., & Gourmelon, F. (2003). Satellite multi-sensor data analysis of urban surface temperatures and land cover. *ISPRS Journal of Photogrammetry and Remote Sensing*, 58, 43–54.
- Geladi, P., & Kowalski, B. R. (1986). Partial least-squares regression: a tutorial. *Analytica Chimica Acta*, 185, 1–17.
- Ge, W.-Q., Zhou, H.-M., & Tu, D.-J. (2005). The surveying on thermal influence area of Shanghai urban greenbelt. *Remote Sensing Technology and Application*, 20, 496–500 (in Chinese).
- Grimm, N.B., Grove, J.M., Pickett, S.T.A., & Redman, C.L. (2000). Integrated approaches to long-term studies of urban ecological systems. *Bioscience*, 50(7), 571–584.
- Grübler, A. (1994). Technology. In W. B. Meyer, & B. L. Turner, II (Eds.), *Changes in land use and land cover: A global perspective* (pp. 287–328). Cambridge: Cambridge University Press.
- Han, S., Bian, H., Tie, X., Xie, Y., Sun, M., & Liu, A. (2009). Impact of nocturnal planetary boundary layer on urban air pollutants: measurements from a 250-m tower over Tianjin, China. *Journal of Hazardous Materials*, 162(1), 264–269.
- Hattis, D., Ogneva-Himmelberger, Y., & Ratnick, S. (2012). The spatial variability of heat-related mortality in Massachusetts. *Applied Geography*, 33, 45–52.
- Hitchcock, D. (3–4 August 2006). Strategic plan for urban heat island mitigation in the Houston Region. In *International workshop on countermeasures to urban heat islands*. Tokyo, Japan.
- Hung, T., Uchiyama, D., Ochi, S., & Yasuoka, Y. (2006). Assessment with satellite data of the urban heat island effects in Asian mega cities. *International Journal of Applied Earth Observation and Geoinformation*, 8, 34–48.
- Jassen, L. I. F., Frans, J. M., & Wel, V. D. (1994). Accuracy assessment of satellite derived land-cover data: a review. *Photogrammetric Engineering & Remote Sensing*, 60, 410–432.
- Jimenez-Munoz, J. C., & Sobrino, J. A. (2003). A generalized single channel method for retrieving land surface temperature from remote sensing data. *Journal of Geophysical Research*, 108(D22), 4688. <http://dx.doi.org/10.1029/2003JD003480>.
- Jin, M., Dickinson, R. E., & Zhang, D.-L. (2005). The footprint of urban areas on global climate as characterized by MODIS. *Journal of Climate*, 18, 1551–1565.
- Johnson, D. P., Stanforth, A., Lulla, V., & Lubet, G. (2012). Developing an applied extreme heat vulnerability index utilizing socioeconomic and environmental data. *Applied Geography*, 35, 23–31.
- Jusuf, S. K., Wong, N. H., Hagen, E., Anggoro, R., & Hong, Y. (2007). The influence of land use on the urban heat island in Singapore. *Habitat International*, 31(2), 232–242.
- Kolokotroni, M., Giannitsaris, I., & Watkins, R. (2006). The effect of the London urban heat island on building summer cooling demand and night ventilation strategies. *Solar Energy*, 80(4), 383–392.
- Landsat Project Science Office. (2002). *Landsat 7 Science data user's handbook*. Goddard Space Flight Center, NASA: Washington, DC. http://ltpwww.gsfc.nasa.gov/LAS/handbook/handbook_toc.html.
- Li, J., & Nin, Y. M. (2007). Population spatial change and urban spatial restructuring in Shanghai since the 1990s. *Urban Planning Forum*, 2, 20–24 (in Chinese).
- Li, F., Jackson, T. J., Kustas, W. P., Schmugge, T. J., French, A. N., Cosh, M. H., et al. (2004). Deriving land surface temperature from Landsat 5 and 7 during SMEX02/SMACEX. *Remote Sensing of Environment*, 92, 521–534.
- Li, Y.-Y., Zhang, H., & Kainz, W. (2012). Monitoring patterns of urban heat islands of the fast-growing Shanghai metropolis, China using time-series of Landsat TM/ETM+ data. *International Journal of Applied Earth Observation and Geoinformation*, 19, 127–138.
- Li, Q., Zhang, H., Liu, X., & Huang, J. (2004). Urban heat island effect on annual mean temperature during the last 50 years in China. *Theoretical and Applied Climatology*, 79(3–4), 165–174.
- Lin, Y.-M., & Bao, K. (2005). The impact of the scan lines corrector malfunction on Landsat-7 imagery data and the processing methods. *Remote Sensing Information*, 2, 33–35 (in Chinese).
- Lo, C. P., & Quattrochi, D. A. (2003). Land-use and land-cover change, urban heat island phenomenon, and health implications: a remote sensing approach. *Photogrammetric Engineering & Remote Sensing*, 69, 1053–1063.
- Malaret, E., Bartolucci, L. A., Lozano, D. F., Anuta, P. E., & McGilllem, C. D. (1985). Landsat-4 and Landsat-5 Thematic Mapper data quality analysis. *Photogrammetric Engineering & Remote Sensing*, 51, 1407–1416.
- Markham, B. L., & Barker, J. L. (1985). Spectral characterization of the Landsat Thematic Mapper sensors. *International Journal of Remote Sensing*, 6, 697–716.
- McCarthy, M. P., Best, M. J., & Betts, R. A. (2010). Climate change in cities due to global warming and urban effects. *Geophysical Research Letters*, 37, L09705.

- Nichol, J. E. (1996). High-resolution surface temperature patterns related to urban morphology in a tropical city: a satellite-based study. *Journal of Applied Meteorology*, 35, 135–146.
- Oke, T. R. (1982). The energetic basis of the urban heat island. *Quarterly Journal of the Royal Meteorological Society*, 108, 1–24.
- Pongrácz, R., Bartholy, J., & Dezso, Z. (2010). Application of remotely sensed thermal information to urban climatology of Central European cities. *Physics and Chemistry of the Earth*, 35, 95–99.
- Qin, Z., Karniel, A., & Berliner, P. (2001). A mono-window algorithm for retrieving land surface temperature from Landsat TM data and its application to the Israel–Egypt border region. *International Journal of Remote Sensing*, 22(18), 3719–3746.
- Rao, P. K. (1972). Remote sensing of urban “heat islands” from an environmental satellite. *Bulletin of the American Meteorological Society*, 53, 647–648.
- Roth, M., Oke, T. R., & Emery, W. J. (1989). Satellite-derived urban heat islands from 3 coastal cities and the utilization of such data in urban climatology. *International Journal of Remote Sensing*, 10, 1699–1720.
- Shalaby, A., & Tateishi, R. (2007). Remote sensing and GIS for mapping and monitoring land cover and land-use changes in the northwestern coastal zone of Egypt. *Applied Geography*, 27, 28–41.
- Shanghai Municipal Commission of Economy and Information. (2008). *Annual report for industrial development in Shanghai-2008* (in Chinese, latest access in December, 2012) <http://www.sheitc.gov.cn/p04010301.htm>.
- Shanghai Municipal Government. (2000). *Master plan of Shanghai city* (in Chinese).
- Shanghai Municipal Government. (2012). *Shanghai's twelfth five-year action plan for energy saving and adaptation to climate change*. Available at <http://www.shanghai.gov.cn/shanghai/node2314/node25307/node25455/node25459/u21ai597380.html> (in Chinese, latest access in November, 2012).
- Shanghai Municipal Statistics Bureau. (2009). *Shanghai statistical yearbook (2009)*. Beijing: China Statistics Press.
- Singh, A. (1989). Digital change detection techniques using remotely sensed data. *International Journal of Remote Sensing*, 10, 989–1003.
- Soleckia, W. D., Rosenzweig, C., Parshall, L., Pope, G., Clark, M., Cox, J., et al. (2005). Mitigation of the heat island effect in urban New Jersey. *Global Environmental Change Part B: Environmental Hazards*, 6(1), 39–49.
- Souch, C., & Grimmond, S. (2006). Applied climatology: urban climatology. *Progress in Physical Geography*, 30, 270–279.
- Srivastava, P. K., Majumdar, T. J., & Bhattacharya, A. K. (2009). Surface temperature estimation in Singhbhum Shear Zone of India using Landsat-7 ETM+ thermal infrared data. *Advances in Space Research*, 43, 1563–1574.
- Stathopoulou, M., & Cartalis, C. (2007). Daytime urban heat islands from Landsat ETM+ and Corine land cover data: an application to major cities in Greece. *Solar Energy*, 81, 358–368.
- Stone, B., Hess, J. J., & Frumkin, H. (2010). Urban form and extreme heat events: are sprawling cities more vulnerable to climate change than compact cities? *Environmental Health Perspectives*, 118, 1425–1428.
- Streutker, D. R. (2003). Satellite-measured growth of the urban heat island of Houston, Texas. *Remote Sensing of Environment*, 85, 282–289.
- Taha, H. (1997). Urban climates and heat islands: albedo, evapotranspiration, and anthropogenic heat. *Energy and Buildings*, 25, 99–103.
- Tan, G. (1994). Potential impacts of global warming on human mortality in Shanghai and Guangzhou, China. *Acta Scientiae Circumstantiae*, 14(3), 368–373 (in Chinese).
- Tang, Q. (2010). *DPS® Data processing system-experimental design, statistical analysis, and data mining* (2nd ed.). Beijing: Science Press.
- Trenberth, K. E., Jones, P. D., Ambenje, P., Bojariu, R., Easterling, D., Tank, A. K., et al. (2007). Observations: surface and atmospheric climate change. In S. Solomon, D. Qin, M. Manning, Z. Chen, M. Marquis, K. B. Averyt, et al. (Eds.), *Climate Change 2007: The Physical Science Basis. Contribution of Working Group I to the Fourth Assessment Report of the Intergovernmental Panel on Climate Change* (pp. 235–336). Cambridge: Cambridge University Press.
- Turner, B. L., II, Lambin, E. F., & Reenberg, A. (2007). The emergence of land change science for global environmental change and sustainability. *Proceedings of the National Academy of Sciences of the United States of America*, 104, 20666–20671.
- United Nations. (2010). *World urbanization prospects: The 2009 revision population database*. <http://esa.un.org/unpd/wup/index.htm>.
- Weng, Q. (2001). A remote sensing-GIS evaluation of urban expansion and its impact on surface temperature in the Zhujiang Delta, China. *International Journal of Remote Sensing*, 22, 1999–2014.
- Xian, G., & Crane, M. (2006). An analysis of urban thermal characteristics and associated land cover in Tampa Bay and Las Vegas using Landsat satellite data. *Remote Sensing of Environment*, 104, 147–156.
- Yamamoto, Y. (2006). Measures to mitigate urban heat islands. *Science and Technology Trends Quarterly Review*, 18, 65–83.
- Yang, J., Gong, P., Zhou, J., Huang, H., & Wang, L. (2010). Detection of urban heat island in Beijing using HJ-1B satellite imagery. *Science in China Series D: Earth Sciences*, 53, 67–73.
- Yow, D. M. (2007). Urban heat islands: observations, impacts, and adaptation. *Geography Compass*, 2, 1227–1251.
- Yue, W., Liu, Y., Ye, X., & Wu, C. (2012). Assessing spatial pattern of urban thermal environment in Shanghai, China. *Stochastic Environmental Research and Risk Assessment*, 26(7), 899–911.
- Zhang, H., Zhou, L., Chen, M., & Ma, W. (2011). Land use dynamics of the fast-growing Shanghai Metropolis, China (1979–2008) and its implications for land use and urban planning policy. *Sensors*, 11(2), 1794–1809.
- Zhou, H. M., Zhou, C. H., Ge, W. Q., & Ding, J. C. (2001). The surveying on thermal distribution in urban based on GIS and remote sensing. *Acta Geographica Sinica*, 56(2), 189–197 (in Chinese).
- Zhou, S.-Z., & Zhang, C. (1985). *Introduction to urban climatology*. Shanghai: Press of East Normal University (in Chinese).